Landslides Data Assimilation Using TRIGRS Based on Particle Filtering

Changhu Xue[1], Guigen Nie[1,2], Jie Dong[3], Shuguang Wu[1], Jing Wang[1], Xiuzhen Li[4], Xiaogang Zhang[4]

[1]GNSS Research Center, Wuhan University, Wuhan, 430079, China
[2]Collaborative Innovation Center for Geospatial Information Technology, Wuhan, 430206, China
[3]State Key Laboratory of Information Engineering in Surveying, Mapping and Remote Sensing, Wuhan University, Wuhan, 430079, China
[4]Institute of Mountain Hazards and Environment, Chinese Academy of Sciences, Chengdu, 610041, China

Correspondence to: Guigen Nie (ggnie@whu.edu.cn)

Abstract. Studies about landslide modeling and monitoring are becoming more diverse. Data assimilation is an approach to combine mechanism models and observations. In this study, an improved particle filtering algorithm is used to assimilate the transient rainfall infiltration and grid-based regional slope-stability analysis (TRIGRS) model and landslide surface deformation monitoring data observed with GPS and InSAR. After assimilation calculation, factor of safety (FS) has been effectively corrected, rather than continuously decreasing as the background model output. The root mean square difference (RMSD) tends to decrease from a maximum of 0.084 to a minimum of 0.026 in the process of assimilation, which means the assimilation process makes the model output FS closer to the actual observations. The friction angle (φ) is an investigated parameter in this experiment, and it can be updated and fed back in each step of assimilation. Parameter update and feedback process make the model prediction trajectory closer to the observation. The groundwater pressure head is output as an assimilation result simultaneously.

1 Introduction

Landslides induced by rainfall pose a huge threat on human lives and properties around the world(Hungr, et al., 2001, Kirschbaum, et al., 2010). Currently, there are varies types of methods for landslides analysis, such as physical mechanism modeling(Wu and Sidle, 1995, Iverson, 2000, Hong, et al., 2007, Baum, et al., 2008, De Blasio and Crosta, 2017, Martelloni, et al., 2017), 3D modeling based on numerical analysis(Crosta, et al., 2003, McDougall and Hungr, 2004, Hungr and McDougall, 2009, Merritt, et al., 2014, Yang, et al., 2014, Martelloni, et al., 2017) and time series analysis of landslide deformation (Gokceoglu and Aksoy, 1996, Hong, et al., 2007, Rossi, et al., 2010, Liu, et al., 2013, Turner, et al., 2015, Dong, et al., 2018). The transient rainfall infiltration and grid-based regional slope-stability analysis (TRIGRS) model program coded in Fortran computes transient pore-pressure changes, and attendant changes in the factor of safety (FS), due to rainfall infiltration. It is designed for modeling the timing and distribution of shallow, rainfall-induced landslides(Baum, et al., 2008). Some studies about landslides safety analysis using TRIGRS are developed in recent years(Liao, et al., 2011, Park, et al., 2013,

Bordoni, et al., 2015, Viet, et al., 2017). Increasing studies about landslide surface deformation monitoring and analysis are carried out, including GNSS, SAR/InSAR technology, three-dimensional laser scanning(Squarzoni, et al., 2005, Brueckl, et al., 2006, Du and Teng, 2007, Peyret, et al., 2008, Yin, et al., 2010, Dong, et al., 2018).

Data assimilation (DA) is a method of combining a dynamic system and observations of its states, in order to improve the accurate description of the system, including its uncertainty analysis. It includes the background model of dynamic process and direct or indirect observations of states. ~~It~~ DA uses all available observed information and background model to simulate the real process, estimate uncertain state and parameters, and thus improve the prediction(Talagrand, 1997, Evensen, 2009). DA is widely applied in many fields such as oceanic and atmospheric modelling for prediction in different scales, regional or global hydrology research including parameter estimation and dynamic analysis, and evolution and inversion of land surface process(Kalnay, et al., 1996, Houtekamer and Mitchell, 2001, Rowley, et al., 2002, Uppala, et al., 2005, Salamon and Feyen, 2009, Plaza, et al., 2012, Mazzoleni, et al., 2018). But in the scope of landslide research, there are only a few preliminary studies(Brezzi, et al., 2016, Jiang, et al., 2016, Xue, et al., 2018). Using the TRIGRS program as the background, we studied the approach to merging observations of landslide surface deformation into the evolutionary model, and investigated the update and feedback of the parameter friction angle (φ).

A great number of approaches of DA have been developed in recent years, of which ~~sequential~~ filtering algorithms like particle filtering (PF) are increasingly popular. PF is ~~based on Bayesian theory and~~ originally introduced by Arulampalam into DA(Arulampalam, et al., 2002). It is developed in many DA studies ~~due to the advantage of being unconstrained by state Gaussian distribution and linear assumptions~~ because that it has the advantage of solving the state estimation problem of nonlinear systems (Weerts and El Serafy, 2006, Chorin, et al., 2010, Liu, et al., 2013, Thirel, et al., 2013, Fearnhead and Kunsch, 2018). However, PF still has disadvantages like particle degradation, which means with the recursion of the system most particles' weights tend to be zero and only a few particles have effects on the results(Carpenter, et al., 1999). Therefore, a number of improved algorithms for particle filtering have been proposed(Pitt and Shephard, 1999, Kotecha and Djuric, 2003, Khan, et al., 2005, van Leeuwen, 2010, Zhang, et al., 2013, Wu, et al., 2014, Xi, et al., 2015).

In this study, an improved particle filter algorithm(Xue, et al., 2018) is adopted to perform assimilation experiments on TRIGRS landslide models and deformation observation data in the area of Xishancun landslide, Sichuan Province, China. InSAR and GPS monitoring data in the study area are chosen as observations of assimilation. Taking friction angle (φ) for example, we investigate the sensitivity analysis to determine the original value of a parameter and propose the parameter update and feedback mechanism to adapt the model to observations. The assimilation results and the ~~change~~ changing trend of friction angle during the assimilation period are illustrated in the paper. Results show that the assimilation can effectively improve the accuracy of state estimation by fixing the TRIGRS model to be close to observations.

2 The improved particle filtering

State transition equations and observation equations for a dynamic space model can be written as

$$\boldsymbol{x}_k = f(\boldsymbol{x}_{k-1}) + \mathbf{G}_k(\boldsymbol{x}_{k-1})\boldsymbol{\varepsilon}_{k-1} \quad (1)$$

$$\boldsymbol{z}_k = h(\boldsymbol{x}_k) + \boldsymbol{\eta}_k \quad (2)$$

where x is the state vector with initial probability density function (PDF) $p(\boldsymbol{x}_0)$, k is the subscript of time steps, $\boldsymbol{\varepsilon}_{k-1}$ is system noise with zero mean at step k-1, and $f(\bullet)$ is the model operator. $\boldsymbol{z}_k$ is the observation vector at step k, and $h(\bullet)$ is the observation operator. In particle filtering, initial N particles are sampled from $p(\boldsymbol{x}_0)$ to express the PDF of the state. The estimation of the state is represented by the weighted average of the particles. Weights of particles are calculated by (3), and normalized to get w_k^i by (4)

$$\tilde{w}_k^i = w_{k-1}^i \cdot \frac{p(z_k \mid x_k^i)\, p(x_k^i \mid x_{k-1}^i)}{q(x_k^i \mid x_{k-1}^i, z_k)} \quad (3)$$

$$w_k^i = \frac{\tilde{w}_k^i}{\sum_{j=1}^{N} \tilde{w}_k^j} \quad (4)$$

where i is the index of particle number, $p(z_k \mid x_k^i)$ is the likelihood of observation, and $q(x_k^i \mid x_{k-1}^i, z_k)$ is the proposal function. The estimation of the state is

$$\hat{x}_{k/k} = \sum_{i=1}^{N} x_k^i \cdot w_k^i \quad (5)$$

An improved particle filtering algorithm was proposed to improve computing efficiency(Xue, et al., 2018). The algorithm made two improvements. Firstly, each particle adds a gain term during the update process to distribute the particle set in the interval where the observed probability density is large. Secondly, with Gaussian-distributed particle sequences are generated to replace replicated particles during resampling so that it can maintain particle diversity. This improved particle filtering algorithm has been proven to improve computational efficiency.

In this experiment, the state transition model is TRIGRS. This process is achieved by updating the parameters, such as shear strength indices and groundwater pressure head. When new observation data is added to update the FS, the parameters are estimated and updated, and then the updated parameters are used for the next operation. Otherwise, the TRIGRS model continues to run and the parameters remain unchanged.

3 Geologic background

The study area is located at around 31°35'N,103°26.5'E (Figure 1), the northern bank of Zagunao River in Xishancun, between Wenchuan and Li County, Sichuan, China. ~~It is at the east of the Tibetan Plateau, where exists a strong crustal activity and influenced by the Wenchuan earthquake in 2008.~~ It is located at the junction of the Eurasian plate and the Indian Ocean

plate. The geological structure is complex and the geological activities are active. The front and rear boundaries are respectively 1510m and 3300m above the sea level. The whole length of the landslide is about 3800m, and the width is varied in a range of 680m to 980m(Qu, et al., 2016). The landslide body is the northern side of a V-shaped valley which is inhabited by a number of villagers, and slides from north to south. Its southern edge is close to Wenma Expressway and National Highway 317. Affected by human activities, such as terraces reclamation and road construction, some areas form severe steep slopes or collapses.

Xishancun Landslide is divided into three parts according to ~~different soil conditions~~ the topography as Figure 2 shows. The slope of the lower block is between 27° to 32°, and the average slope of the middle block and upper block are 22° and 27° respectively. The middle block has a part of thick and loose soil, and the deformation is relatively large. The deformations of lower and upper blocks are relatively small. Due to the highest resolution of the observed data is 5 meters, the landslide is divided into 781×477 grids, part of the surrounding area included. Distribution of soil thickness and groundwater depth in the grid is shown in Figure 3.

4 Data observation and processing

Several GPS stations and boreholes are established on the surface of Xishancun Landslide. Four GPS monitoring stations are receiving positioning observations along the sliding direction of the landslide body. One base station is established on the bedrock of the adjacent mountain, monitoring the three-dimensional deformation of the landslide surface by relative positioning. Three boreholes are distributed in each block to obtain hydrological parameters of different areas. Figure 4 shows the positions of GPS stations and boreholes on the slope.

4.1 ~~Collection of~~ Deformation Observations

GPS Monitoring data is collected from Aug 12, 2015, to Nov 07, 2017, one set of observations every 10 days. In order to eliminate the influence of plate motion, we use the relative positioning method to calculate the displacement of each monitoring station related to the base station (Figure 4). Correspondingly, the relative positioning error sequence is as shown in Figure 5. Another data set is InSAR observations of Sentinel-1 interferometric wide (Sentinel-1 IW) data. The Sentinel-1 IW image width is 250km, and each image consists of three left and right overlapping frames. We collect the Sentinel-1 IW data for the period of Aug 5, 2015, to Jul 13, 2017, a total of 34 sets of data. Most of these data sets are separated by 12 or 24 days and a few by 6 days. InSAR observation accuracy is usually better than 1cm. An average velocity map of deformations per-year is illustrated in Figure 7. However, the displacement of InSAR observation is always along the direction of the radar line of sight (LOS). In order to verify the consistency of GPS and InSAR observations, these two observations must be projected in the same direction. The conversion vector of GPS 3D-displacement projection to the line of sight is $[-0.13 \quad 0.58 \quad 0.80]$. ~~InSAR~~

~~observations have been corrected for atmospheric delays to reduce fluctuations.~~ We select the displacement of the InSAR observation with a radius of 50 meters around the GPS station and compare it with the GPS observing results. Sequences of ~~corrected~~ InSAR and projected GPS observations are displayed in figure 8. As we can see, the two observing results are consistent in both trend and quantity in most circumstances. InSAR monitoring points are distributed throughout the landslide surface, but the distribution is uneven and does not coincide with GPS stations. So we put InSAR points and the GPS points into the grid, and some areas where the observation data is sparse are supplemented by interpolation. According to the post-failure movement model of a landslide triggered by rainfall infiltration, the relationship between FS and displacement rate is expressed as

$$\frac{1}{g}\frac{dv}{dt} = \sin\alpha[1 - FS] \tag{2}$$

where g is the magnitude of gravity acceleration, α is the slope angle(Iverson, 2000). The observed velocities can be converted into FS using formula (2) when the slope is slipping. Therefore, the converted FS can be used as a set of observations for sensitivity analysis and assimilation experiment.

4.2 ~~Sensitivity analysis~~ Hydrological data

Statistics of boreholes in the landslide are collected, including data of instruments such as inclinometer, pore water pressure gauge, and soil hygrometer are installed in each borehole.

The rainfall data was obtained by bilinear interpolation from the China Ground Meteorological Information Center (http://data.cma.cn), “China Ground Precipitation 0.5°×0.5° Grid Data Set (V2.0)”. Hydraulic conductivity calculated by the recording speed of the drawdown standpipe. Hydraulic parameters such as saturated soil water content, soil bulk density, are obtained by collecting local geotechnical samples.

One parameter can be estimated according to the observation data. Due to the dynamic change of shear strength determines the equilibrium state of the soil, we choose the shear strength indicators as parameters for the real-time update. ~~The initial value and trend of some parameters in landslide evolution are usually difficult to exactly determine.~~ Before the process of data assimilation, sensitivity analysis is necessary to determine the initial values of shear strength indicators. In this work, ~~friction angle (φ), is selected to conduct the sensitivity analysis.~~ the shear strength of the soil is changed by changing the internal friction angle to calculate the value that matches the observed data. Other parameters ~~are fixed~~ remain unchanged while the ~~friction angle~~ shear strength ~~is adjusted from minimum to maximum~~ investigated. Since the true value of FS is unknown, and the accuracy of the observations is relatively high, we compare the assimilation results with observations. The root means square difference (RMSD) of all grid cells is used as the evaluation of ~~sensitivity analysis~~ matching.

$$RMSD_k = \sqrt{\frac{1}{N_p}\sum_{i,j}(FS_{ij}(\varphi_k) - FS_{ij}^{obs})^2} \tag{3}$$

where $FS(\varphi)$ is the FS calculated by TRIGRS program using parameter φ, FS^{obs} is the converted FS from GPS/InSAR observations, N_p is the total number of grid points, i, j are row and column number, respectively. ~~Figure 7 shows the RMSD sequences of the 3 landslide blocks calculated by sensitivity analysis of φ. The result shows that the model is best performed when initial friction angles of 3 blocks are~~ 19.2°, 22.0°, 22.2° ~~, respectively.~~

4.3 Assimilation experiment

In order to facilitate the realization of the experiment, the FS is used as an assimilation variable for one-dimensional data assimilation experiments. The assimilation experiment starts on the first day of observation data and occurs daily using the improved PF. If there is observation data on the current day, the assimilation is performed, otherwise, only the model recursion is performed. The friction angle is updated at the same time of each assimilating calculation with formula (4).

$$\hat{\varphi}_k = \sum_{i=1}^{N} \varphi_k^i \cdot w_k^i \tag{4}$$

in which $\hat{\varphi}_k$ is the estimation of φ at step k, φ_k^i is the ith sample of φ in particle filtering, w^i is the corresponding sample weight.

The FS results of background model and assimilation output are illustrated in figure 9. Compared with the model output, there is a significant change in the safety factor after assimilation. In the background of the TRIGRS program, the only changing parameter is rainfall, so the model output results have small fluctuations and gently decreases with time. Assimilation results are more dependent on observations. Correction of FS after assimilation relative to the model output is shown in figure 10, and it shows the distribution and change of assimilation corrections. As the assimilation progresses, the correction amount shows an increasing trend. This is because the model prediction error accumulates and its deviation from the actual value is getting larger. After statistics, all grid results after assimilation with Fs less than 1.0 are closer to the observed value than the model results.

Figure 11 shows sequences of model output and assimilated results of three grid cells randomly selected from Block I, II, III, respectively. It can be seen that the change tracks of FS are corrected by observations obviously. Since rainfall is the only variable input parameter in the background model, the TRIGRS output FS sequences present relatively stable downward trends. Although significant fluctuations are obvious in observations and are propagated into assimilation results, the assimilation series has been significantly improved. The RMSD sequence of assimilation output FS on the whole landslide calculated by the formula (3) is shown in figure 12. Its maximum value is 0.084 at the second step of assimilation, and the minimum is 0.026 in the last several steps. Overall, with the assimilation proceeding, the RMSD of results tends to become smaller and its sequence gradually becomes stable.

The friction angle (φ) is a parameter to be investigated in this experiment, so the distribution and the changes are displayed in figure 13 and time series of the 3 grid cells are shown in figure 14. In the assimilation progresses, the change of the internal friction angle is mainly affected by the actual soil water content and deviation of other initial parameters.

Convert the assimilated FS into annual average deformation rate using formula (1), its distribution map is as figure 15 (a) shows. Figure 15 (b) is the observed deformation rate map. Groundwater pressure head (ψ) is an important parameter in slope stability analysis. In this experiment, ψ is also considered as an output parameter. Figure 16 demonstrates the distribution of ψ and its change with assimilation time. The ψ time series of the above 3 points and the rainfall sequence is illustrated in figure 17. There is a certain correlation between rainfall and pressure head series, and the correlation coefficients of the three points are 0.384, 0.323 and 0.314. They exhibit a medium correlation because the correlation coefficient is also affected by the variance of the observed data, and the experimental observation data variance is relatively large.

5 Conclusion and discussion

Data assimilation is a method that can combine mechanism models with observational data. In data assimilation fields, particle filtering is becoming increasingly popular since it can help to solve non-linear and non-Gaussian problems efficiently. In this study, data assimilation with ~~an improved~~ particle filtering algorithm is applied to landslide model and observation data processing. TRIGRS model is used as the background, GPS and InSAR monitoring data as input observation in the experiment. Results suggest that the fs sequence of TRIGRS output decreases continuously with time and the assimilation can effectively correct the FS of the model output so that it does not deviate too much from the actual. The RMSD of FS indicates the assimilation results can correct the estimation of TRIGRS output close to actual observations. The experiment also examined the changes of soil friction angle and the groundwater pressure head which can help to analyze the soil water content and slope stability in the landslide body.

This paper provides an approach to apply data assimilation method to stability analysis and parameter update and feedback in a landslide. Landslide data assimilation experiments have many directions for further research, such as better mathematical models, more comprehensive and high-precision observations, and more excellent assimilation algorithms.

Data availability. The InSAR data of Sentinel-1 is downloaded from Alaska Satellite Facility: https://www.asf.alaska.edu/sentinel/. GPS data is collected from the field, and the observation sequence is uploaded in the supplement. The model information and program of TRGIRS are obtained from https://pubs.usgs.gov/of/ 2008/1159/ (US Geological Survey, 2017).

Author contributions. CX conceived the idea of this article and completed the paper. GN helped to solve some important problems and proposed some key suggestions. JD provided the data analysis of GPS/InSAR. SW and JW made contributions to the validation of the algorithm, chart sorting, and editing. XL and XZ helped to build the model with the TRIGRS program.

Competing interests. The authors declare that they have no conflict of interest.

Acknowledgments. This work is financially supported by the National Key Basic Research Program of China (grant no. 2013CB733205).

References

Arulampalam, M. S., Maskell, S., Gordon, N., and Clapp, T.: A tutorial on particle filters for online nonlinear/non-Gaussian Bayesian tracking, Ieee T Signal Proces, 50, 2, 174-188, doi: 10.1109/78.978374, 2002.

Baum, R. L., Savage, W. Z., and Godt, J. W.: TRIGRS—A Fortran Program for Transient Rainfall Infiltration and Grid-Based Regional Slope-Stability Analysis, version 2.0, 2008–1159, 75, doi: 2008.

Bordoni, M., Meisina, C., Valentino, R., Bittelli, M., and Chersich, S.: Site-specific to local-scale shallow landslides triggering zones assessment using TRIGRS, Nat Hazard Earth Sys, 15, 5, 1025-1050, doi: 10.5194/nhess-15-1025-2015, 2015.

Brezzi, L., Bossi, G., Gabrieli, F., Marcato, G., Pastor, M., and Cola, S.: A new data assimilation procedure to develop a debris flow run-out model, Landslides, 13, 5, 1083-1096, doi: 10.1007/s10346-015-0625-y, 2016.

Brueckl, E., Brunner, F. K., and Kraus, K.: Kinematics of a deep-seated landslide derived from photogrammetric, GPS and geophysical data, 88, 3-4, 149-159, doi: 10.1016/j.enggeo.2006.09.004, 2006.

Carpenter, J., Clifford, P., and Fearnhead, P.: Improved particle filter for nonlinear problems, Iee P-Radar Son Nav, 146, 1, 2-7, doi: 10.1049/ip-rsn:19990255, 1999.

Chorin, A., Morzfeld, M., and Tu, X. M.: Implicit Particle Filters for Data Assimilation, Comm App Math Com Sc, 5, 2, 221-240, doi: 10.2140/camcos.2010.5.221, 2010.

Crosta, G. B., Imposimato, S., and Roddeman, D. G.: Numerical modelling of large landslides stability and runout, Nat. Hazards Earth Syst. Sci., 3, 6, 523-538, doi: 10.5194/nhess-3-523-2003, 2003.

De Blasio, F. V. and Crosta, G. B.: Modelling Martian landslides: dynamics, velocity, and paleoenvironmental implications, Eur Phys J Plus, 132, 11, doi: 10.1140/epjp/i2017-11727-x, 2017.

Dong, J., Zhang, L., Tang, M. G., Liao, M. S., Xu, Q., Gong, J. Y., and Ao, M.: Mapping landslide surface displacements with time series SAR interferometry by combining persistent and distributed scatterers: A case study of Jiaju landslide in Danba, China, Remote Sens Environ, 205, 180-198, doi: 10.1016/j.rse.2017.11.022, 2018.

Dong, J., Zhang, L., Li, M. H., Yu, Y. H., Liao, M. S., Gong, J. Y., and Luo, H.: Measuring precursory movements of the recent Xinmo landslide in Mao County, China with Sentinel-1-and ALOS-2 PALSAR-2 datasets, Landslides, 15, 1, 135-144, doi: 10.1007/s10346-017-0914-8, 2018.

Du, J.-C. and Teng, H.-C.: 3D laser scanning and GPS technology for landslide earthwork volume estimation, 16, 5, 657-663, doi: 10.1016/j.autcon.2006.11.002, 2007.

Evensen, G.: The Ensemble Kalman Filter for Combined State and Parameter Estimation MONTE CARLO TECHNIQUES FOR DATA ASSIMILATION IN LARGE SYSTEMS, Ieee Contr Syst Mag, 29, 3, 83-104, doi: 10.1109/Mcs.2009.932223, 2009.

Fearnhead, P. and Kunsch, H. R.: Particle Filters and Data Assimilation, Annu Rev Stat Appl, 5, 421-449, doi: 10.1146/annurev-statistics-031017-100232, 2018.

Gokceoglu, C. and Aksoy, H.: Landslide susceptibility mapping of the slopes in the residual soils of the Mengen region (Turkey) by deterministic stability analyses and image processing techniques, Eng. Geol., 44, 1-4, 147-161, doi: 10.1016/s0013-7952(97)81260-4, 1996.

Hong, Y., Adler, R., and Huffman, G.: Use of satellite remote sensing data in the mapping of global landslide susceptibility, Nat Hazards, 43, 2, 245-256, doi: 10.1007/s11069-006-9104-z, 2007.

Houtekamer, P. L. and Mitchell, H. L.: A sequential ensemble Kalman filter for atmospheric data assimilation, Mon Weather Rev, 129, 1, 123-137, doi: 10.1175/1520-0493(2001)129<0123:asekff>2.0.co;2, 2001.

Hungr, O. and McDougall, S.: Two numerical models for landslide dynamic analysis, Comput. Geosci., 35, 5, 978-992, doi: 10.1016/j.cageo.2007.12.003, 2009.

Hungr, O., Evans, S. G., Bovis, M. J., and Hutchinson, J. N.: A review of the classification of landslides of the flow type, Environ Eng Geosci, 7, 3, 221-238, doi: 10.2113/gseegeosci.7.3.221, 2001.

Iverson, R. M.: Landslide triggering by rain infiltration, Water Resour Res, 36, 7, 1897-1910, doi: Doi 10.1029/2000wr900090, 2000.

Jiang, Y. A., Liao, M. S., Zhou, Z. W., Shi, X. G., Zhang, L., and Balz, T.: Landslide Deformation Analysis by Coupling Deformation Time Series from SAR Data with Hydrological Factors through Data Assimilation, Remote Sens-Basel, 8, 3, doi: 10.3390/rs8030179, 2016.

Kalnay, E., Kanamitsu, M., Kistler, R., Collins, W., Deaven, D., Gandin, L., Iredell, M., Saha, S., White, G., Woollen, J., Zhu, Y., Chelliah, M., Ebisuzaki, W., Higgins, W., Janowiak, J., Mo, K. C., Ropelewski, C., Wang, J., Leetmaa, A., Reynolds, R., Jenne, R., and Joseph, D.: The NCEP/NCAR 40-year reanalysis project, Bull. Amer. Meteorol. Soc., 77, 3, 437-471, doi: 10.1175/1520-0477(1996)077<0437:tnyrp>2.0.co;2, 1996.

Khan, Z., Balch, T., and Dellaert, F.: MCMC-based particle filtering for tracking a variable number of interacting targets, IEEE Trans. Pattern Anal. Mach. Intell., 27, 11, 1805-1819, doi: 10.1109/tpami.2005.223, 2005.

Kirschbaum, D. B., Adler, R., Hong, Y., Hill, S., and Lerner-Lam, A.: A global landslide catalog for hazard applications: method, results, and limitations, Nat Hazards, 52, 3, 561-575, doi: 10.1007/s11069-009-9401-4, 2010.

Kotecha, J. H. and Djuric, P. A.: Gaussian particle filtering, IEEE Trans. Signal Process., 51, 10, 2592-2601, doi: 10.1109/tsp.2003.816758, 2003.

Liao, Z. H., Hong, Y., Kirschbaum, D., Adler, R. F., Gourley, J. J., and Wooten, R.: Evaluation of TRIGRS (transient rainfall infiltration and grid-based regional slope-stability analysis)'s predictive skill for hurricane-triggered landslides: a case study in Macon County, North Carolina, Nat Hazards, 58, 1, 325-339, doi: 10.1007/s11069-010-9670-y, 2011.

Liu, P., Li, Z. H., Hoey, T., Kincal, C., Zhang, J. F., Zeng, Q. M., and Muller, J. P.: Using advanced InSAR time series techniques to monitor landslide movements in Badong of the Three Gorges region, China, Int J Appl Earth Obs, 21, 253-264, doi: 10.1016/j.jag.2011.10.010, 2013.

Martelloni, G., Bagnoli, F., and Guarino, A.: A 3D model for rain-induced landslides based on molecular dynamics with fractal and fractional water diffusion, Commun Nonlinear Sci, 50, 311-329, doi: 10.1016/j.cnsns.2017.03.014, 2017.

Mazzoleni, M., Chacon-Hurtado, J., Noh, S. J., Seo, D. J., Alfonso, L., and Solomatine, D.: Data Assimilation in Hydrologic Routing: Impact of Model Error and Sensor Placement on Flood Forecasting, J Hydrol Eng, 23, 6, doi: 10.1061/(Asce)He.1943-5584.0001656, 2018.

McDougall, S. and Hungr, O.: A model for the analysis of rapid landslide motion across three-dimensional terrain, Can. Geotech. J., 41, 6, 1084-1097, doi: 10.1139/t04-052, 2004.

Merritt, A. J., Chambers, J. E., Murphy, W., Wilkinson, P. B., West, L. J., Gunn, D. A., Meldrum, P. I., Kirkham, M., and Dixon, N.: 3D ground model development for an active landslide in Lias mudrocks using geophysical, remote sensing and geotechnical methods, Landslides, 11, 4, 537-550, doi: 10.1007/s10346-013-0409-1, 2014.

Park, D. W., Nikhil, N. V., and Lee, S. R.: Landslide and debris flow susceptibility zonation using TRIGRS for the 2011 Seoul landslide event, Nat Hazard Earth Sys, 13, 11, 2833-2849, doi: 10.5194/nhess-13-2833-2013, 2013.

Peyret, M., Djamour, Y., Rizza, M., Ritz, J. F., Hurtrez, J. E., Goudarzi, M. A., Nankali, H., Chery, J., Le Dortz, K., and Uri, F.: Monitoring of the large slow Kahrod landslide in Alborz mountain range (Iran) by GPS and SAR interferometry, 100, 3-4, 131-141, doi: 10.1016/j.enggeo.2008.02.013, 2008.

Pitt, M. K. and Shephard, N.: Filtering via simulation: Auxiliary particle filters, J Am Stat Assoc, 94, 446, 590-599, doi: Doi 10.2307/2670179, 1999.

Plaza, D. A., De Keyser, R., De Lannoy, G. J. M., Giustarini, L., Matgen, P., and Pauwels, V. R. N.: The importance of parameter resampling for soil moisture data assimilation into hydrologic models using the particle filter, Hydrol Earth Syst Sc, 16, 2, 375-390, doi: 10.5194/hess-16-375-2012, 2012.

Qu, T. T., Lu, P., Liu, C., Wu, H. B., Shao, X. H., Wan, H., Li, N., and Li, R. X.: Hybrid-SAR Technique: Joint Analysis Using Phase-Based and Amplitude-Based Methods for the Xishancun Giant Landslide Monitoring, Remote Sens-Basel, 8, 10, doi: 10.3390/rs8100874, 2016.

Rossi, M., Witt, A., Guzzetti, F., Malamud, B. D., and Peruccacci, S.: Analysis of historical landslide time series in the Emilia-Romagna region, northern Italy, 35, 10, 1123-1137, doi: 10.1002/esp.1858, 2010.

Rowley, C., Barron, C., Smedstad, L., and Rhodes, R.: Real-time ocean data assimilation and prediction with global NCOM, Oceans 2002 Mts/Ieee Conference & Exhibition, Vols 1-4, Conference Proceedings, 775-780, 2002.

Salamon, P. and Feyen, L.: Assessing parameter, precipitation, and predictive uncertainty in a distributed hydrological model using sequential data assimilation with the particle filter, J Hydrol, 376, 3-4, 428-442, doi: 10.1016/j.jhydrol.2009.07.051, 2009.

Squarzoni, C., Delacourt, C., and Allemand, P.: Differential single-frequency GPS monitoring of the La Valette landslide (French Alps), Eng Geol, 79, 3-4, 215-229, doi: 10.1016/j.enggeo.2005.01.015, 2005.

Talagrand, O.: Assimilation of observations, an introduction, J Meteorol Soc Jpn, 75, 1b, 191-209, doi: 10.2151/jmsj1965.75.1B_191, 1997.

Thirel, G., Salamon, P., Burek, P., and Kalas, M.: Assimilation of MODIS Snow Cover Area Data in a Distributed Hydrological Model Using the Particle Filter, Remote Sens-Basel, 5, 11, 5825-5850, doi: 10.3390/rs5115825, 2013.

Turner, D., Lucieer, A., and de Jong, S. M.: Time Series Analysis of Landslide Dynamics Using an Unmanned Aerial Vehicle (UAV), Remote Sens-Basel, 7, 2, 1736-1757, doi: 10.3390/rs70201736, 2015.

Uppala, S. M., Kallberg, P. W., Simmons, A. J., Andrae, U., Bechtold, V. D., Fiorino, M., Gibson, J. K., Haseler, J., Hernandez, A., Kelly, G. A., Li, X., Onogi, K., Saarinen, S., Sokka, N., Allan, R. P., Andersson, E., Arpe, K., Balmaseda, M. A., Beljaars, A. C. M., Van De Berg, L., Bidlot, J., Bormann, N., Caires, S., Chevallier, F., Dethof, A., Dragosavac, M., Fisher, M., Fuentes, M., Hagemann, S., Holm, E., Hoskins, B. J., Isaksen, L., Janssen, P., Jenne, R., McNally, A. P., Mahfouf, J. F., Morcrette, J. J., Rayner, N. A., Saunders, R. W., Simon, P., Sterl, A., Trenberth, K. E., Untch, A., Vasiljevic, D., Viterbo, P., and Woollen, J.: The ERA-40 re-analysis, Q. J. R. Meteorol. Soc., 131, 612, 2961-3012, doi: 10.1256/qj.04.176, 2005.

van Leeuwen, P. J.: Nonlinear data assimilation in geosciences: an extremely efficient particle filter, Q J Roy Meteor Soc Q J Roy Meteor Soc, 136, 653, 1991-1999, doi: 2010.

Viet, T. T., Lee, G., Thu, T. M., and An, H. U.: Effect of Digital Elevation Model Resolution on Shallow Landslide Modeling Using TRIGRS, Nat Hazards Rev, 18, 2, doi: 10.1061/(Asce)Nh.1527-6996.0000233, 2017.

Weerts, A. H. and El Serafy, G. Y. H.: Particle filtering and ensemble Kalman filtering for state updating with hydrological conceptual rainfall-runoff models, Water Resour Res, 42, 9, doi: 10.1029/2005wr004093, 2006.

Wu, W. M. and Sidle, R. C.: A Distributed Slope Stability Model for Steep Forested Basins, Water Resour Res, 31, 8, 2097-2110, doi: 10.1029/95wr01136, 1995.

Wu, Y., Wang, J., and Zhang, P. C.: Least-squares particle filter, Electron Lett, 50, 24, 1881-U249, doi: 10.1049/el.2014.2980, 2014.

Xi, Y. H., Peng, H., Kitagawa, G., and Chen, X. H.: The auxiliary iterated extended Kalman particle filter, Optim Eng, 16, 2, 387-407, doi: 10.1007/s11081-014-9266-6, 2015.

Xue, C., Nie, G., Li, H., and Wang, J.: Data assimilation with an improved particle filter and its application in the TRIGRS landslide model, 18, 10, 2801-2807, doi: 10.5194/nhess-18-2801-2018, 2018.

Yang, Q. Q., Cai, F., Su, Z. M., Ugai, K. Z., Xu, L. Y., Huang, R. Q., and Xu, Q.: Numerical Simulation of Granular Flows in a Large Flume Using Discontinuous Deformation Analysis, Rock Mech Rock Eng, 47, 6, 2299-2306, doi: 10.1007/s00603-013-0489-1, 2014.

Yin, Y., Zheng, W., Liu, Y., Zhang, J., and Li, X.: Integration of GPS with InSAR to monitoring of the Jiaju landslide in Sichuan, China, 7, 3, 359-365, doi: 10.1007/s10346-010-0225-9, 2010.

Zhang, H. J., Qin, S. X., Ma, J. W., and You, H. J.: Using Residual Resampling and Sensitivity Analysis to Improve Particle Filter Data Assimilation Accuracy, Ieee Geosci Remote S, 10, 6, 1404-1408, doi: 10.1109/Lgrs.2013.2258888, 2013.

Figures

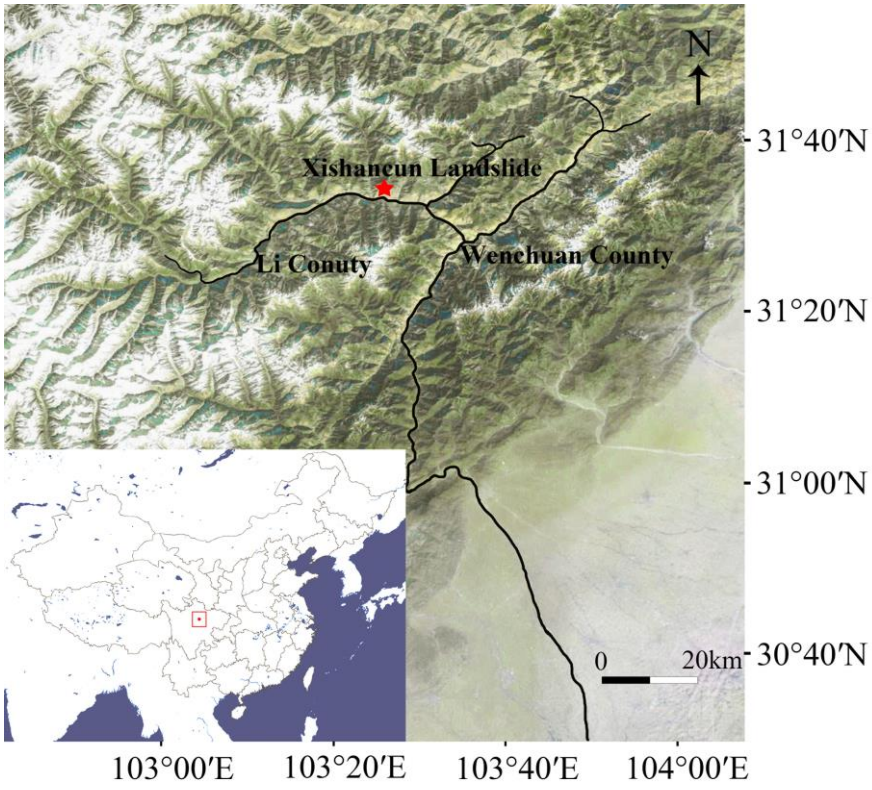

Figure 1. Location of Xishancun Landslide in the red rectangle and its location in China.

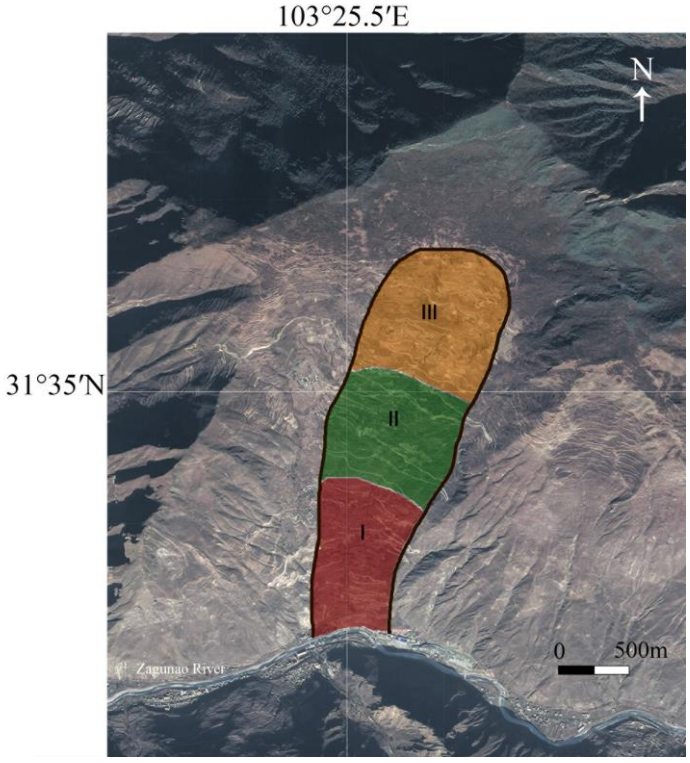

Figure 2. The top view and blocks of the study area.

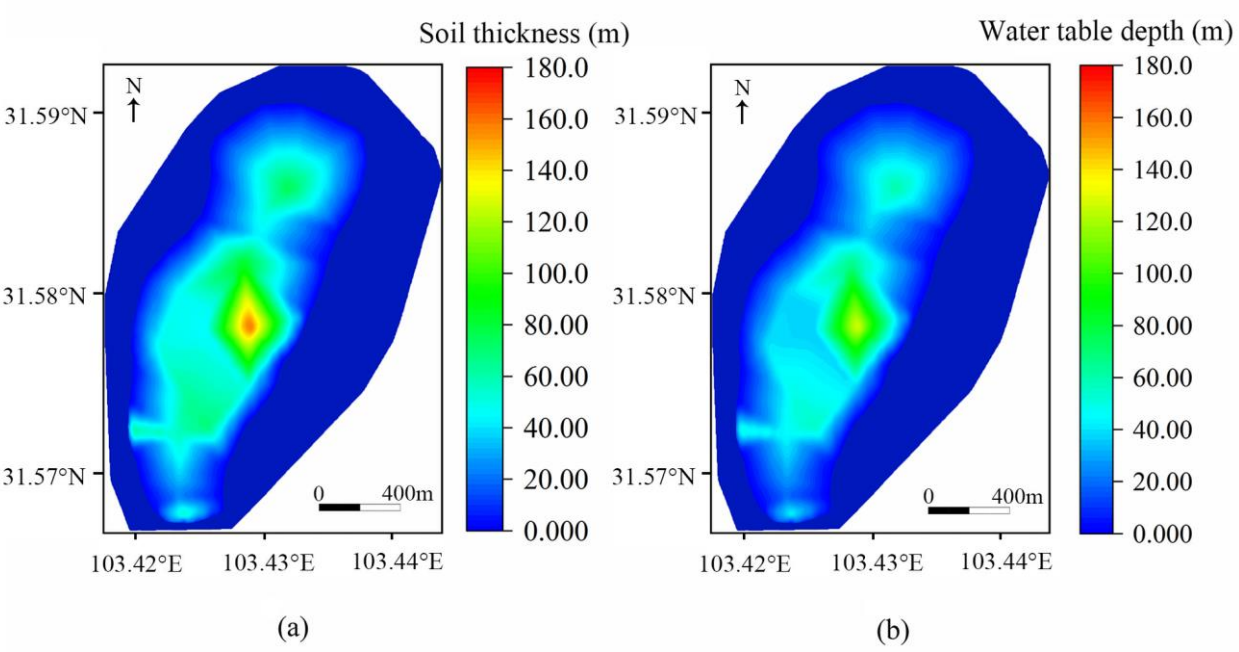

Figure 3. Distribution of soil thickness and groundwater depth in the grid. (a) shows the soil thickness of the landslide, (b) shows the groundwater depth. The x-axis and y-axis represent the number of columns and the number of rows, respectively.

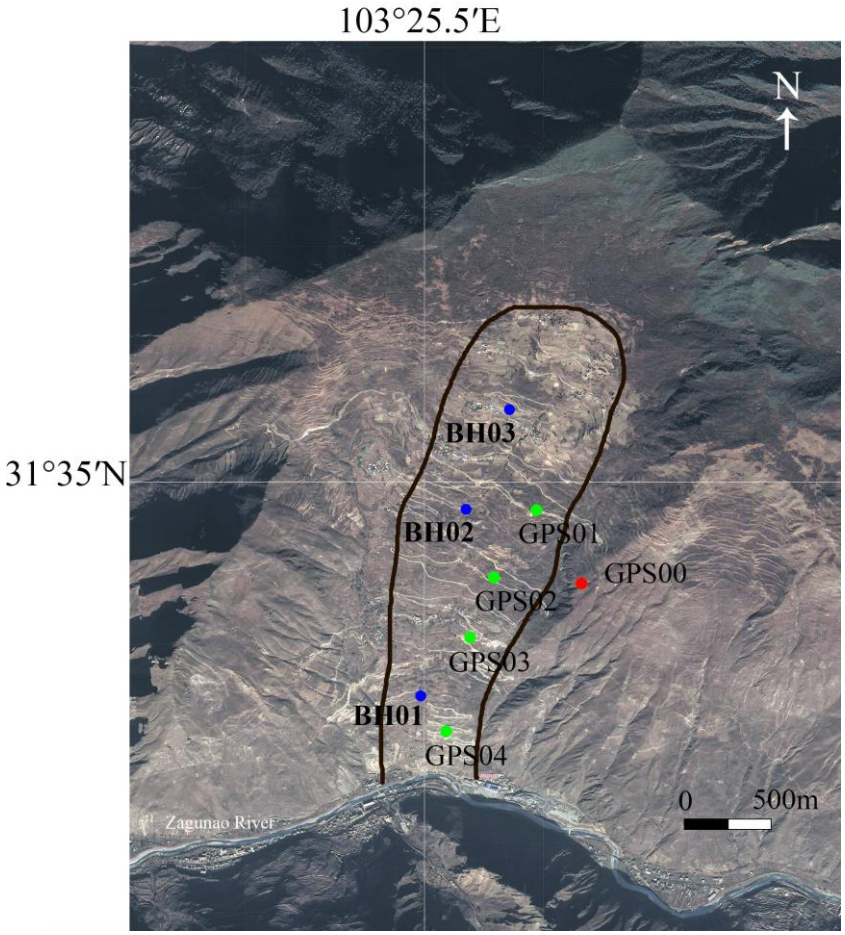

Figure 4. Location map of GPS monitoring stations and boreholes. GPS01-GPS04 are monitoring stations on the landslide surface, GPS00 is the base station built on bedrock. BH01-BH03 are boreholes.

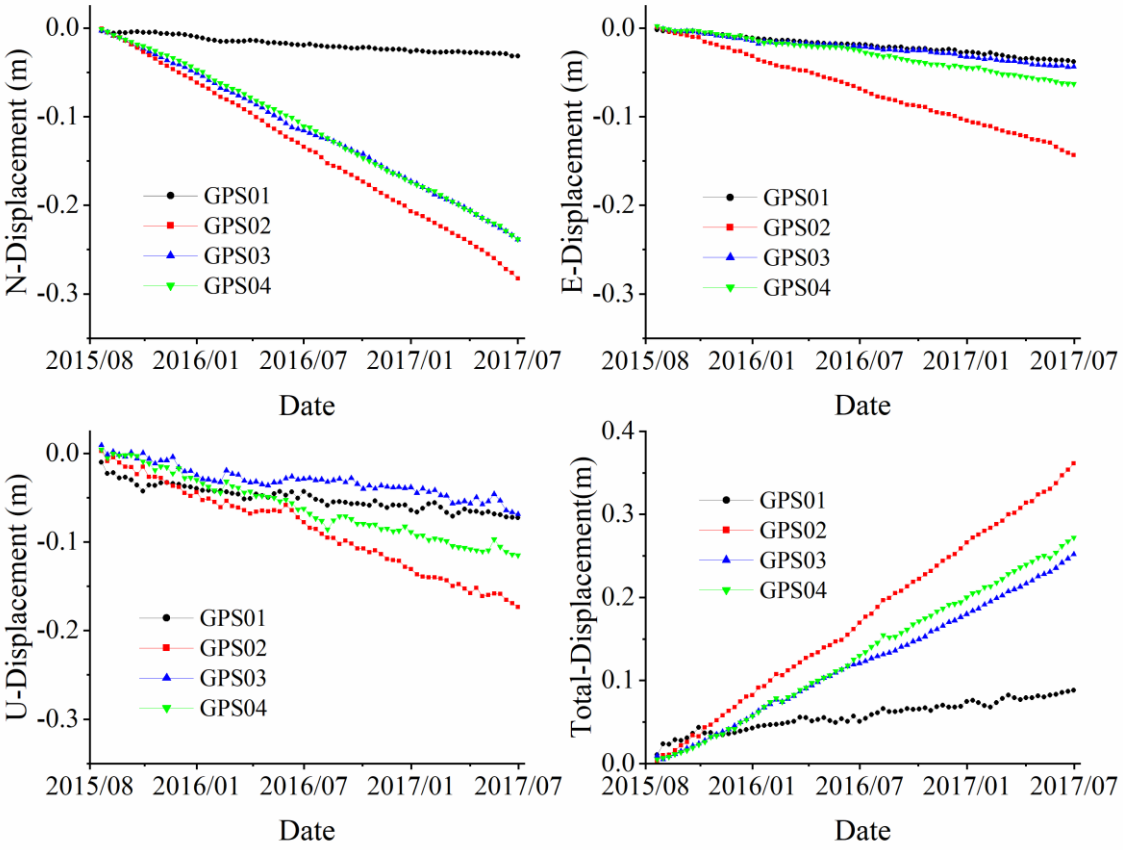

Figure 5. Displacement series of the 4 GPS monitoring stations. (a), (b) and (c) are the figures of displacements in the north, east and upper directions respectively, (d) is the total displacements figure.

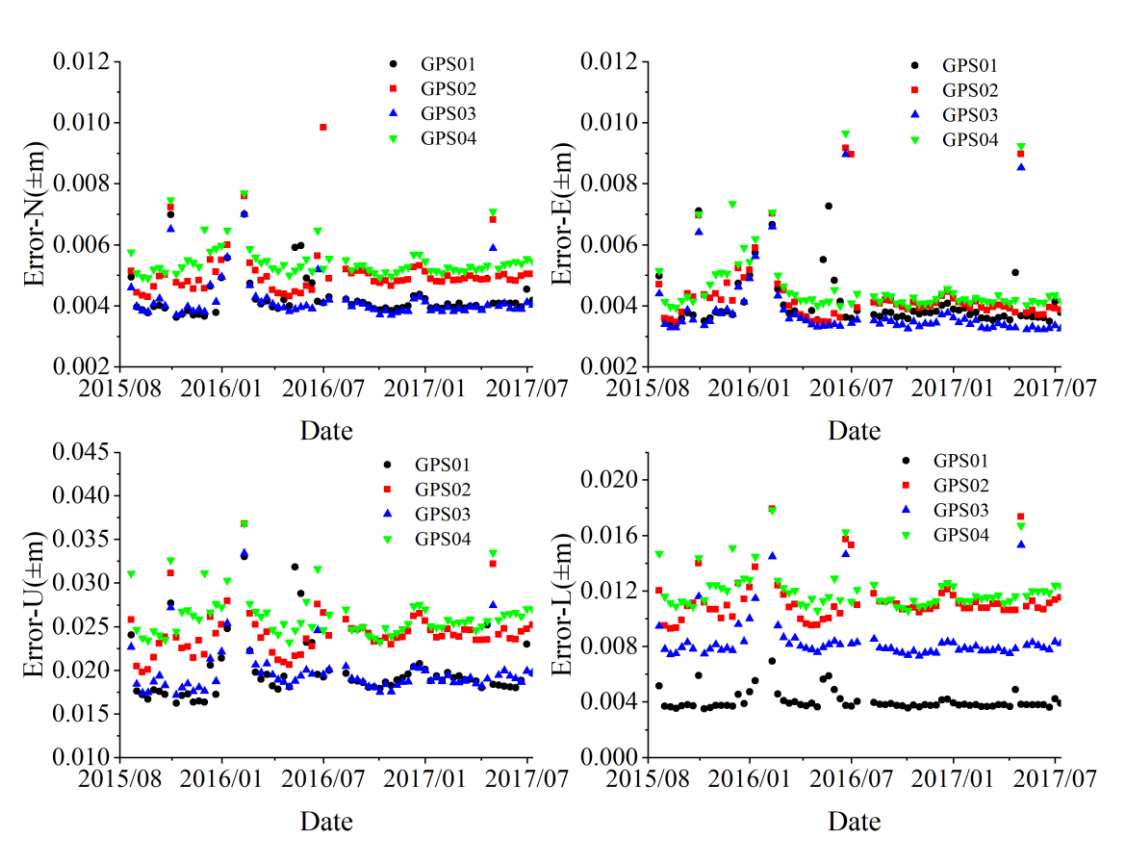

Figure 6. Errors in relative positioning of GPS monitoring points in N, E, U and baseline directions.

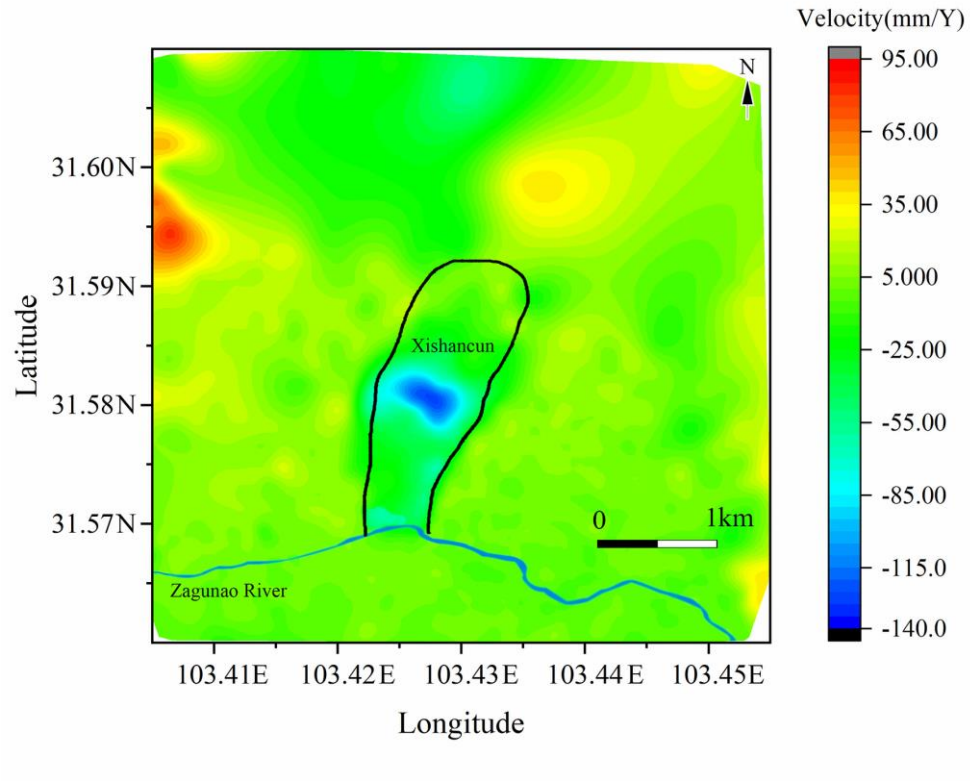

Figure 7. Displacement rate map of Xishancun area monitored by Sentinel-1 data.

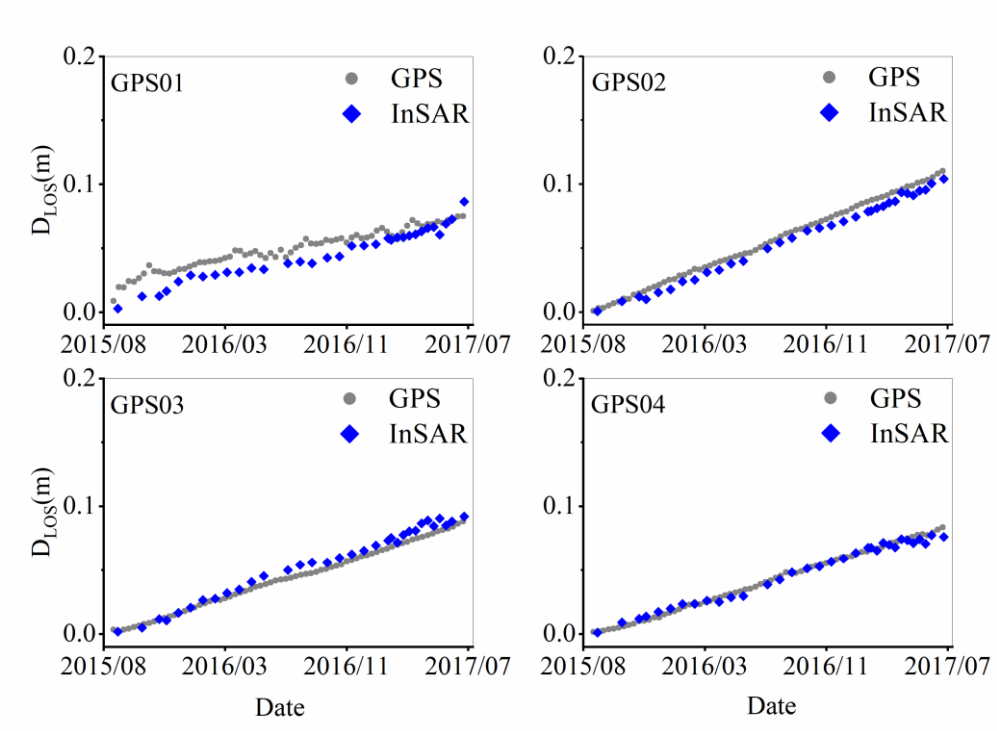

Figure 8. Comparison of GPS and INSAR monitoring displacement sequences in LOS direction.

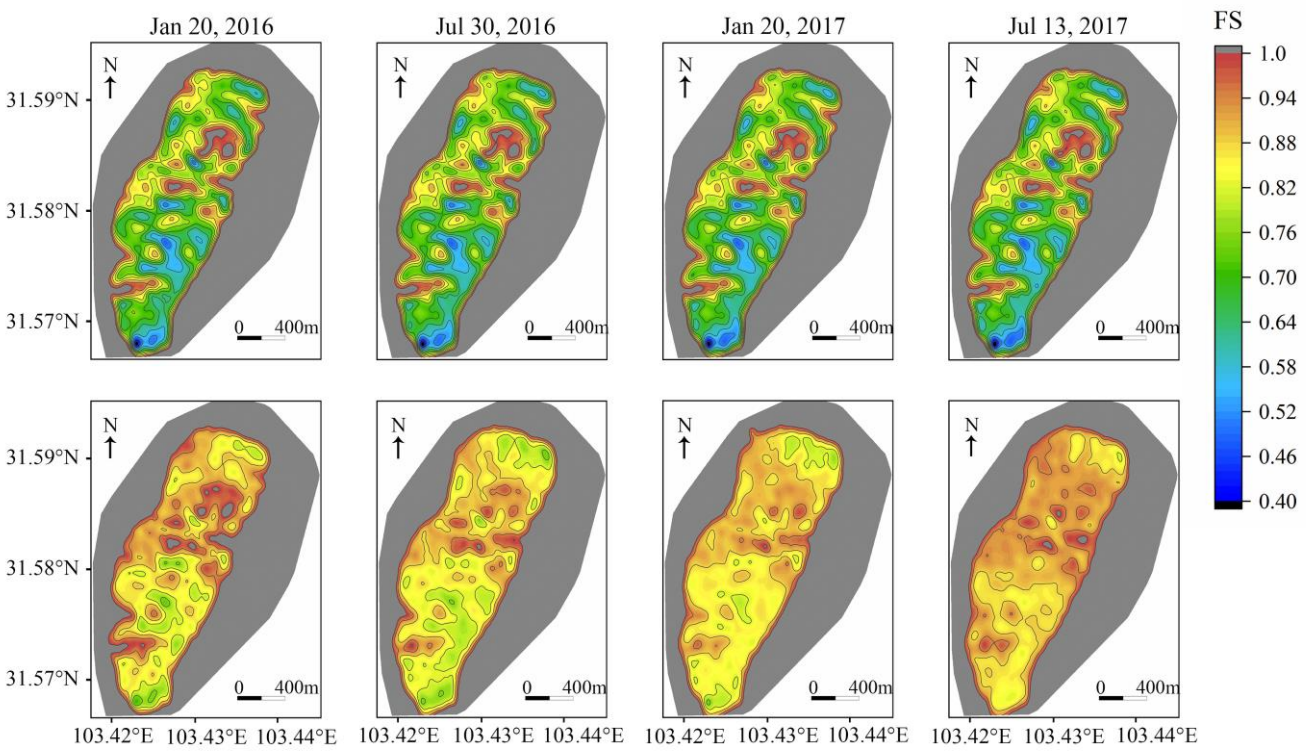

Figure 9. Comparison of background model output results and assimilation results. The maps in the first line are TRIGRS output results, and those in the second line are assimilation results.

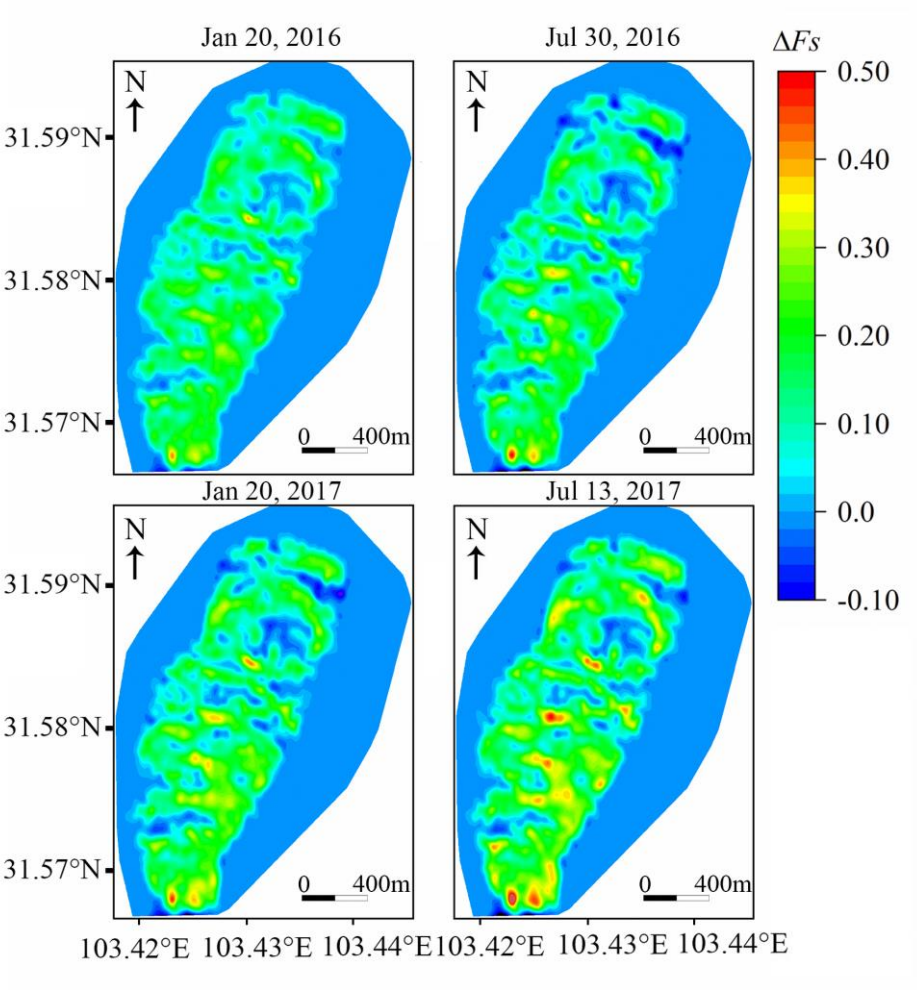

Figure 10. Correction of FS after assimilation relative to the model output.

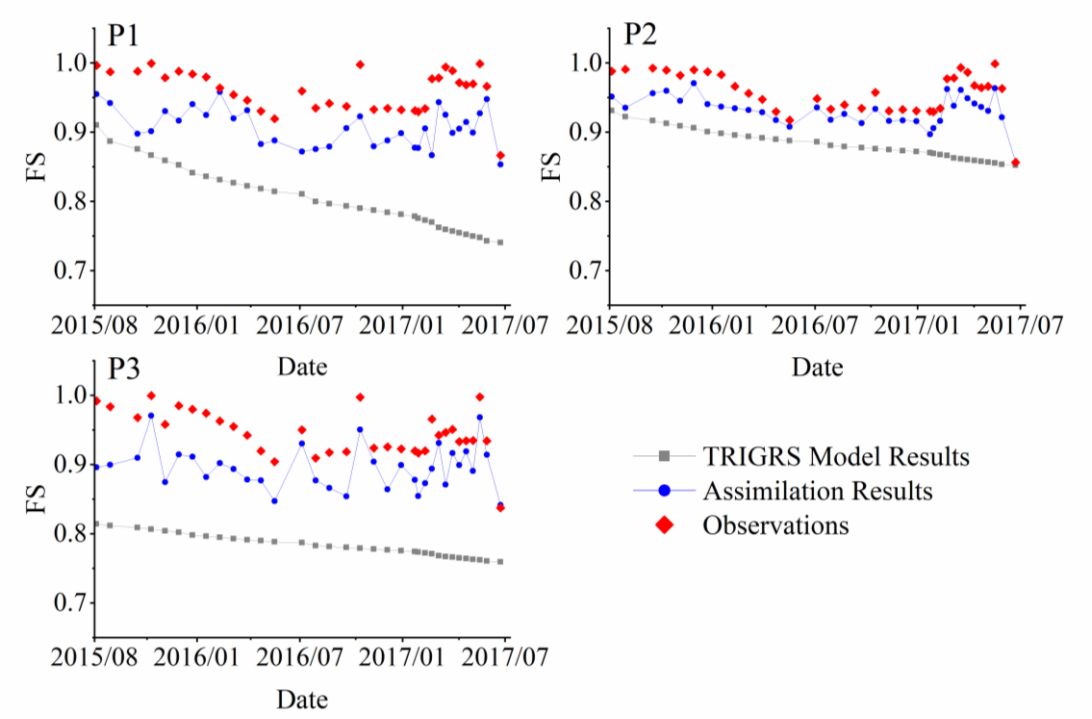

Figure 11. Model and assimilation sequences of 3 points selected from Block I, II, III, respectively.

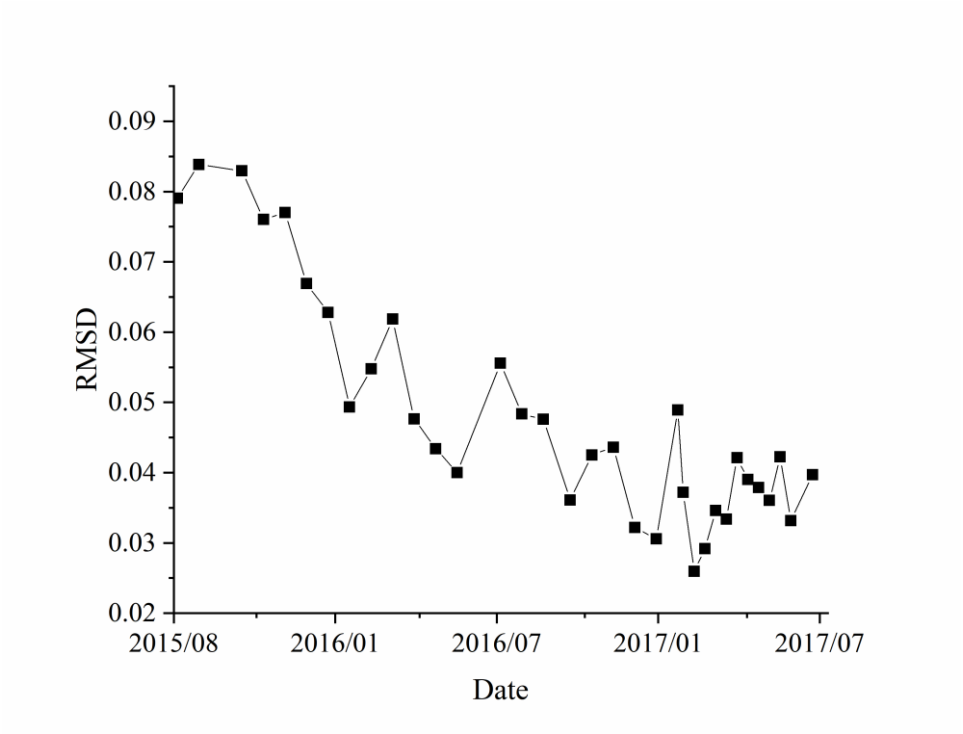

Figure 12. The RMSD sequence of assimilation output FS related on observations.

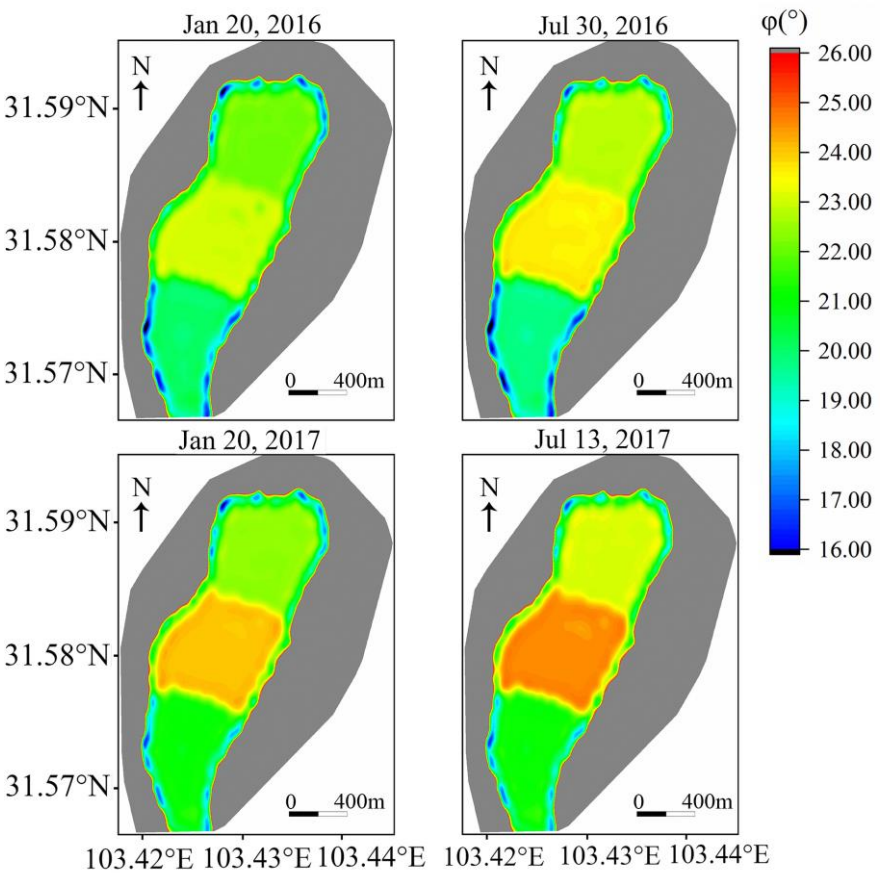

Figure 13. The distribution of friction angle and its change with assimilation time. There are obvious boundaries in the distribution map because the TRIGRS program divides different blocks into zones.

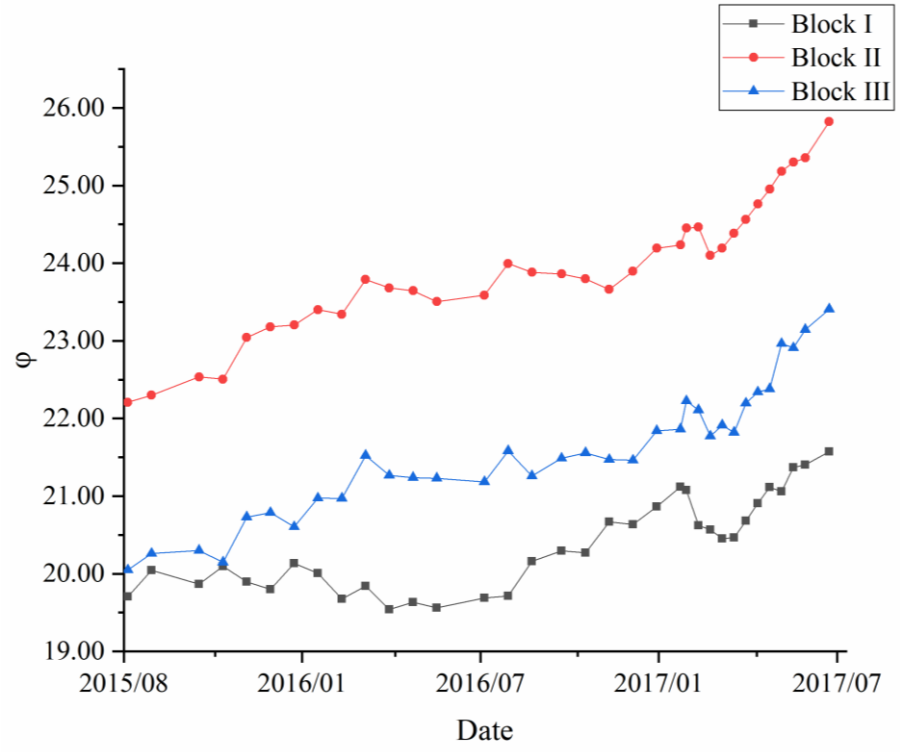

Figure 14. Friction angle time series of three points after assimilation.

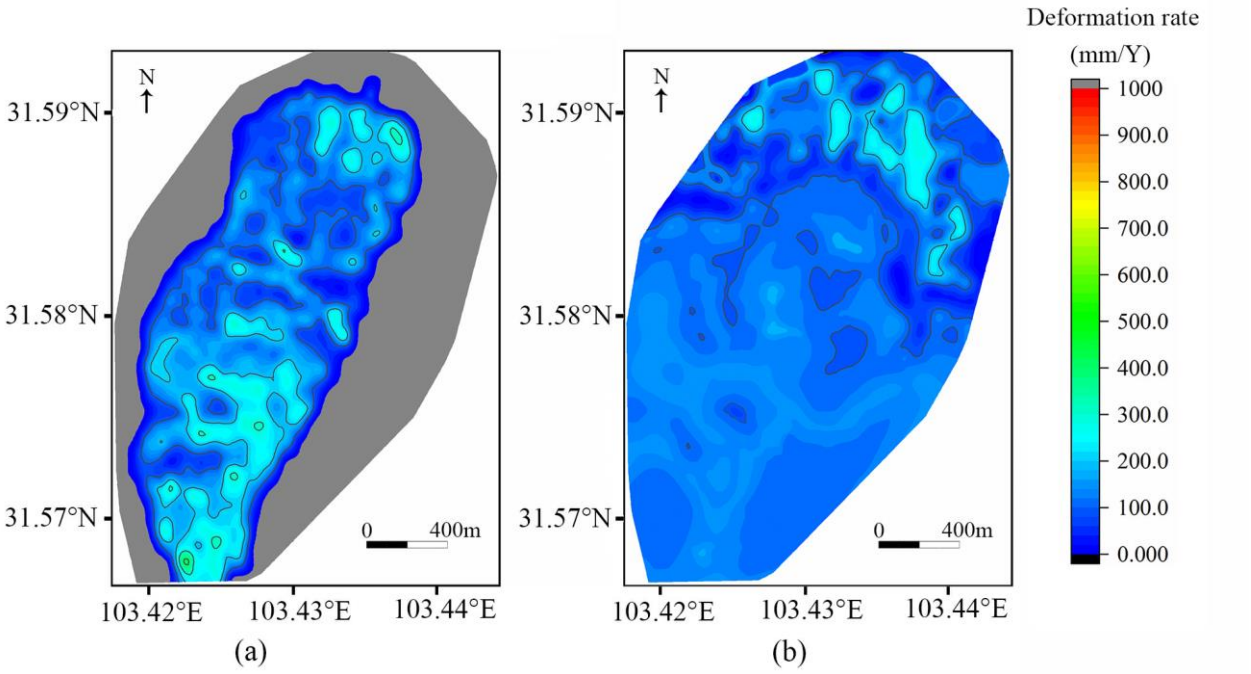

Figure 15. Distributions of annual deformation rate: (a) Calculated by the assimilated FS (Landslide area); (b) Observed deformation results (Observation coverage area).

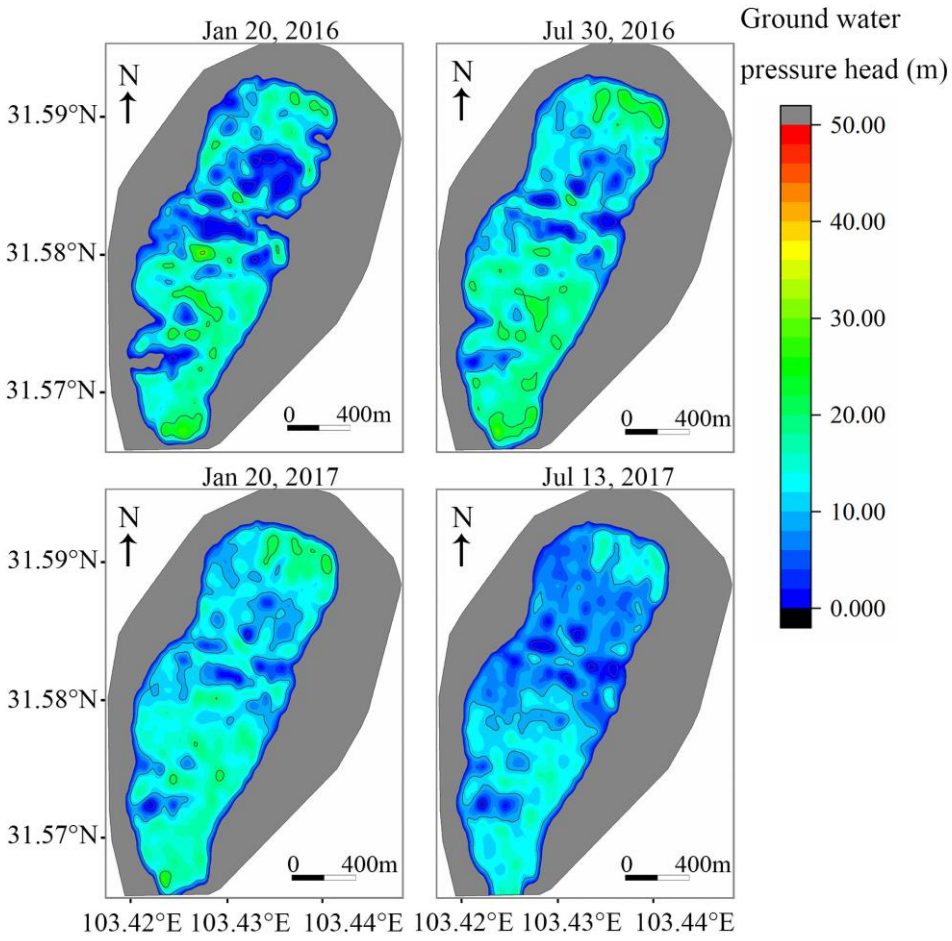

Figure 16. The distribution of groundwater pressure head and its change with time.

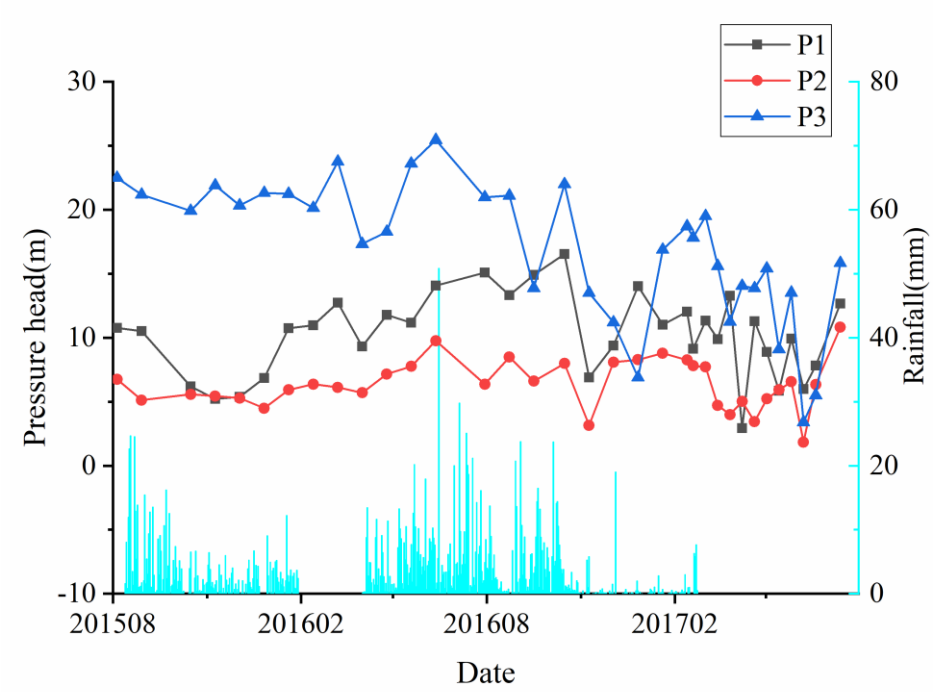

Figure 17. The groundwater pressure head time series of the three points and accumulated rainfall sequence.